

# The Role of HiPIMS Pulse Length in Reactive Deposition of Transparent Conductive Oxide Nb:TiO<sub>2</sub> Films

J. Stryhalski<sup>a,b\*</sup> , A. Laur<sup>a</sup>, J.C. Sagás<sup>c</sup> , A.A Couto<sup>a</sup> , K. Grigorov<sup>a</sup> , L.C. Fontana<sup>c</sup> , M. Massi<sup>a</sup> 

<sup>a</sup>Universidade Presbiteriana Mackenzie, São Paulo, SP, Brasil.

<sup>b</sup>Instituto Federal de Santa Catarina, Florianópolis, SC, Brasil.

<sup>c</sup>Universidade do Estado de Santa Catarina, Joinville, SC, Brasil.

Received: November 29, 2022; Revised: May 05, 2023; Accepted: May 21, 2023

The present paper sets out to investigate the role of voltage pulse length on the properties of Nb:TiO<sub>2</sub> films deposited by High Power Impulse Magnetron Sputtering (HiPIMS). Several characteristics of the films were investigated, namely, resistivity, transmittance, crystallinity and band gap values of Nb:TiO<sub>2</sub> films. Reactive depositions were carried out in Ar/O<sub>2</sub> plasma with 40 μs, 50 μs, 60 μs, and 70 μs pulses. Increasing the pulse length changes the deposition from compound to metal mode. As it gets closer to metal mode, the deposition rate increases by up to one order of magnitude, while the resistivity of the resulting Nb:TiO<sub>2</sub> film becomes as low as 10<sup>-4</sup> Ω.cm, without any significant loss in optical transmittance, which remains close to 90% for a wavelength around 450 nm, but reduction in 25% of heat transmission (above 800 nm) were observed. Results indicate the anatase phase for all deposition conditions, and Ti<sup>3+</sup> states increase with the pulse length, which can be explained by the generation of a second band gap. Both the niobium doping and the Ti<sup>3+</sup> states can contribute to increase the conductivity of the Nb:TiO<sub>2</sub> films in the as-deposited condition.

**Keywords:** Titanium dioxide, Niobium, Resistivity, Optical properties, HiPIMS.

## 1. Introduction

Niobium-doped TiO<sub>2</sub> (Nb:TiO<sub>2</sub>) has been quoted as a promising indium-free transparent conducting oxide material (TCO), as a photocatalyst in water purification, and as a self-cleaning coating for glass windows<sup>1,2</sup>. Different methods have been used to deposit doped TiO<sub>2</sub> films, such as RF and pulsed sputtering<sup>3</sup>. Nowadays, reactive HiPIMS (R-HiPIMS) is a successful method to produce compound films, despite its low deposition rate in comparison to direct current magnetron sputtering (DCMS). The low deposition rate in HiPIMS systems has been mainly attributed to a high current of metal ions returning to the target. However, such current can produce a beneficial hysteresis reduction effect, thus providing a higher stability in the deposition process as discussed by Gudmundsson et al.<sup>4</sup>. Kadlec and Čapek<sup>5</sup> show that the discharge current is also influenced by other aspects, namely, the target material, the secondary electron emission, multiple charged metal ions and the gas rarefaction effect<sup>5</sup>. In Lundin work, the magnitude of such variables depends on the operating mode (metal or poisoned) which may be controlled through the “voltage pulse length” provided by the HiPIMS power supply<sup>6</sup>. Different strategies have been used to increase the deposition rate, improve the stoichiometry and control coverage capability<sup>7</sup>. Controlling the voltage pulse waveform, rather than the flow of reactive gas, can be more effective to control the deposition mode, and the film stoichiometry in an R-HiPIMS system<sup>8</sup>. Anders,<sup>9</sup> argued that adjusting the reactive gas partial pressure close to the transition region allows to identify the change from “poisoned” to “metal”

mode, and vice-versa, by a very significant variation in the plasma current. For DC Pulsed Magnetron Sputtering, the process could be stabilized by controlling the partial pressure, for example. However, in R-HiPIMS, the pulse length is an easily manageable parameter which can be used to control the poisoning state of the target. Its control can provide a gradual and stable transition from poisoned target to quasi-metallic or metal deposition mode<sup>10</sup>. For example, the literature indicates that appropriate selections of pulse lengths make the reactive deposition of HfO<sub>2</sub> by R-HiPIMS in metal mode possible, increasing the deposition rate without the need for an active regulation of oxygen flow<sup>11</sup>. Similar conclusions were reached by other authors in experiments aiming to deposit optically transparent, high-refractive-index Nb<sub>2</sub>O<sub>5</sub> films using R-HiPIMS<sup>8</sup>. Given that, the present paper sets out to investigate the role of the pulse length (40 μs to 70 μs) on the compound to metal mode transition and its effects on Nb:TiO<sub>2</sub> film properties. Resulting Nb:TiO<sub>2</sub> films showed good crystallinity in the as-deposited condition, without the need for any post-annealing for film crystallization, as found in previous works in the literature<sup>12,13</sup>. In addition, the films show a 10<sup>-4</sup> Ω.cm resistivity keeping high transmittance of around 90% in visible region, with 25% of reduction of transmittance above 800 nm that is important for facades of buildings, hence, Nb:TiO<sub>2</sub> films are also a potential candidate for heat-filtering applications.

## 2. Experimental Details

Nb:TiO<sub>2</sub> films were deposited on glass substrates through HiPIMS operating at a constant peak voltage.

\*e-mail: joel@ifsc.edu.br

The HiPIMS voltage pulse length were 40  $\mu\text{s}$ , 50  $\mu\text{s}$ , 60  $\mu\text{s}$ , and 70  $\mu\text{s}$  (-660 V), with a fixed frequency of 600 Hz (corresponding to a period of 1.67 ms) resulting in duty-cycles of 2.4%, 3.0%, 3.6%, and 4.2% respectively.

The deposition parameters are shown in Table 1. Four niobium rods ( $\varnothing = 2$  mm) were symmetrically inserted into the erosion zone of a Ti target (99.9%) in order to produce an Nb-doped TiO<sub>2</sub> film.

The films were characterized through X-ray diffraction ( $\lambda = 1.54$  nm) in a diffractometer Shimadzu XRD 600. Measurements were obtained in the range of 20.00° to 70.00° with an increment of 0.02°, using a voltage of 40 kV and a current of 30 mA. The scanning rate was fixed at 2.0° per minute. Optical transmission and specular reflection spectra at wavelengths ranging from 200 nm to 1400 nm were performed in Shimadzu UV-2600 PC spectrophotometer equipped with an integrating sphere. The optical data were used to estimate the optical gaps ( $E_g$ ) through Tauc plots<sup>14</sup>. The resistivity of Nb:TiO<sub>2</sub> deposited on glass substrate were measured through a Hall Effect equipment with d.c. four-probe method in the Van der Pauw electrode configuration<sup>15</sup>. The resistivity and the Hall voltages were measured using a Keithley nanovoltmeter with sensitivity up to 1 V in a magnetic field of 1 T generated by an electromagnet. The electric current source was provided by a Keithley 2410 source meter with a sensitivity range of 1  $\mu\text{A}$  to 1 A. All the measurements were carried out under atmospheric pressure and at room temperature. A region on the glass substrate was covered with a silicon fillet during deposition, resulting in a step between the region without and with silicon. This was used to assess the thin film thickness which was measured using Atomic Force Microscope (AFM) ToscaTM 400 by Anton Paar.

The chemical state was determined through X-ray photoelectron spectroscopy (XPS) in a Thermo Scientific K-Alpha system. High-resolution spectra of the Ti 2p region were acquired with an energy step size of 0.10 eV, a pass energy of 50.00 eV, and a dwell time of 50 ms. Each of these spectra is an average of 5 scans. In all cases, the X-ray spot was 400  $\mu\text{m}$ . A flood gun was used to avoid sample surface charging. All spectra were charge-corrected to the C 1s peak of adventitious carbon at 284.80 eV.

### 3. Results and Discussions

Figure 1 shows square-shaped 40  $\mu\text{s}$ , 50  $\mu\text{s}$ , 60  $\mu\text{s}$  and 70  $\mu\text{s}$  long voltage pulses (-660 V), and the respective discharge current. The current waveform in reactive HiPIMS is determined by the type of ion recycling that dominates the discharge. For a HiPIMS discharge in an Ar/O<sub>2</sub> atmosphere with a Ti target, Gudmundsson<sup>4</sup> showed that, in metal mode, the discharge is dominated by self-sputter ion recycling, which leads to an upper limit in the current and a plateau shape for the current waveform, as observed in Figure 1 for a pulse length of 70  $\mu\text{s}$ . On the other hand, in the poisoned mode, the discharge is dominated by working gas ion recycling, and the absence of an upper limit of discharge current results in a triangular shape<sup>4</sup>, as observed for 40  $\mu\text{s}$  and 50  $\mu\text{s}$ . So, increasing the pulse length shifts the deposition from compound to metal mode.

Table 2 shows the film thickness for different pulse lengths. Besides the lower current for 70  $\mu\text{s}$  pulses, the deposition rate increases by one order of magnitude when compared to shorter pulses. A high discharge current can be associated with the target poisoning. On the other hand, a lower current, in addition to a high deposition rate, can be associated with metallic mode sputtering, which is observed for longer pulses in the present paper. This may be a consequence of gas rarefaction next to the target, once the long pulse could heat the gas in front of it, but the exact mechanism is not well known<sup>16</sup>. The sputter yield in R-HiPIMS processes for oxides and metals is complex as it involves numerous factors such as type of ions, electron density, composition of neutral and ionized atoms self-sputtering, and working gas recycling<sup>4,17</sup>.

**Table 1.** Plasma deposition parameters.

Deposition Parameters	
Target to substrate	6.0 cm
Ar flow rate	86 sccm
O <sub>2</sub> flow rate	2.5 sccm
Ultimate pressure	10 <sup>-5</sup> Torr (~10 <sup>-3</sup> Pa)
Working pressure	5.0 mTorr (0.66 Pa)
Target voltage	-660 V
Average power at target ( $\varnothing 2^\circ$ )	130 W
Frequency	600 Hz
Substrate temperature	200 °C
Substrate Bias	-30 VDC
Deposition time	1 h

**Table 2.** Thickness of films for different pulse lengths.

T <sub>pulse</sub>	40 $\mu\text{s}$	50 $\mu\text{s}$	60 $\mu\text{s}$	70 $\mu\text{s}$
Thickness $\pm 5$ (nm)	55	78	107	548

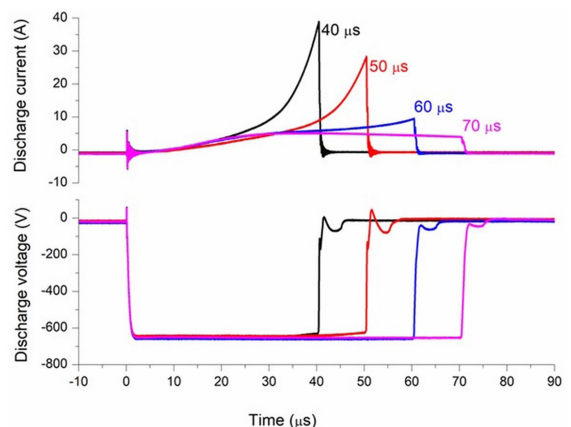


**Figure 1.** Target voltage and current waveforms for pulse lengths of 40  $\mu\text{s}$ , 50  $\mu\text{s}$ , 60  $\mu\text{s}$ , and 70  $\mu\text{s}$ .

XRD and Transmittance results performed on samples are shown in Figure 2 and Figure 3, respectively. The XRD patterns (COD-9008213) indicate the growing of the anatase TiO<sub>2</sub> phase, planes (011) (020) and (121). The (011) peak becomes less intense as the voltage pulse increases from 40  $\mu$ s to 70  $\mu$ s. The reduction of the XRD peaks may be correlated to partially amorphous Nb:TiO<sub>2</sub> and titanium suboxides (TiO<sub>x</sub>). No peaks associated with niobium phases were detected, which suggest that niobium atoms are in substitutional sites into the TiO<sub>2</sub> crystal lattice or it is in amorphous phase.

Transmittance curves (Figure 3) are shifted to larger wavelengths as the pulses increase from 40  $\mu$ s to 70  $\mu$ s. Despite the larger thickness ( $\sim$  550 nm) of the film deposited with a 70  $\mu$ s pulse, the transmittance reaches 90% at a 450 nm wavelength. The transmittance in the infrared range (around 800 nm) drops from  $\approx$  90% (non-coated sample) to  $\approx$  65% (Nb:TiO<sub>2</sub> coated samples). The transmittance of Nb:TiO<sub>2</sub> coated samples is also about 20% lower than glass coated with non-doped TiO<sub>2</sub> films (anatase phase), when compared with values from the literature<sup>18</sup>. Hence, Nb:TiO<sub>2</sub> films are also a potential candidate for heat-filtering applications.

In general, the transmittance decreases as the thickness increases. This is because a thicker material will interact more with the light, resulting in the occurrence of multiple reflections and a higher likelihood of absorption in thin films with non-homogeneous or columnar growth, as described by Equation 1<sup>19</sup>:

$$ad = 1n \left( \frac{T}{1-R} \right) \quad (1)$$

In this study, the transmittance (T) and reflectance (R) of the films were measured, and the absorption coefficient ( $\alpha$ ) was determined based on the known film thickness (d) to access band gap energy. The reflectance is low along the evaluated wavelength and the absorption depends on the electronic transition energy of the material. The optical absorption of anatase occur in the ultraviolet wavelength range at an absorption edge between 300 and 400 nm. Above 400 nm the anatase absorption coefficient is very low, as shown by<sup>20</sup>

The absorption of lower energy photons in the infrared range happens primarily through weakly-bound electrons available to move through the crystalline structure<sup>19</sup>, which, when in appropriate quantity, keep the transmittance of bulk-like glass and anatase TiO<sub>2</sub>. On the other hand, below 400 nm, there is a shift in the falling edge of transmittance. The 80% transmittance region has a blue-shift from 345 nm for the uncoated glass to 410 nm in the 70  $\mu$ s condition, indicating a reduction in the band gap and an improvement in UV absorption. This UV photon absorption is performed primarily by bound electrons and determine the band gap energy<sup>19</sup>.

Semiconducting materials can exhibit a direct or indirect band-to-band transition depending on their electronic structure. Both types of transitions can be observed in the same material<sup>21,22</sup>. Some authors have indicated that, in TiO<sub>2</sub>, the anatase has an indirect band gap of 3.2 eV<sup>23</sup>, while Figure 4 clearly shows that the indirect anatase band gap  $E_{g1}$  had a clear Burstein-Moss shift of 0.3 eV in all samples<sup>24-26</sup>.

This is explained by the fact that the extra electrons from the Nb replacing the Ti populate states within the conduction band, which pushes the Fermi level to a higher energy that can explain  $E_{g1} \approx 3,5$  eV.

Optical transitions in semiconductors involve localized states in the band gap that can be changed when they are doped. The doping can add electrons to the conduction band of oxides, which can behave like free electrons or even cause a lattice distortion induced by their presence (electron-phonon interaction), forming the so called polaronic states<sup>27</sup>. The doping-generated charge carriers interact with the lattice energy states and locally distort the lattice, which can lead to the formation of in-gap states<sup>28</sup>. That can significantly change electrical and optical properties, including an observed second energy gap that decreases from 3.19 eV to 2.80 eV with an increasing deposition pulse length. This second band gap can be associated with the Ti<sup>3+</sup> states identified in the XPS, which will be better explained later. However, this hypothesis needs to be further investigated.

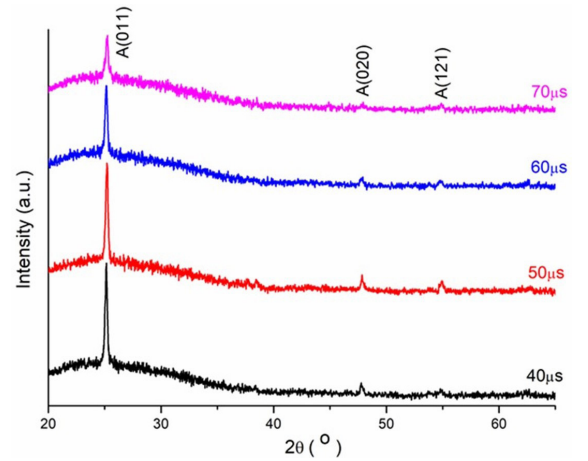


Figure 2. XRD pattern for 40  $\mu$ s, 50  $\mu$ s, 60  $\mu$ s and 70  $\mu$ s pulses.

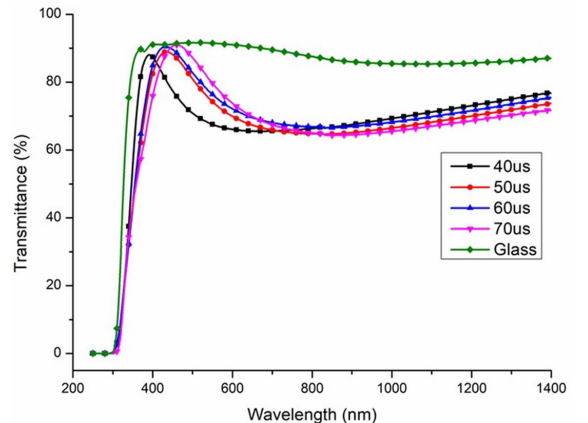


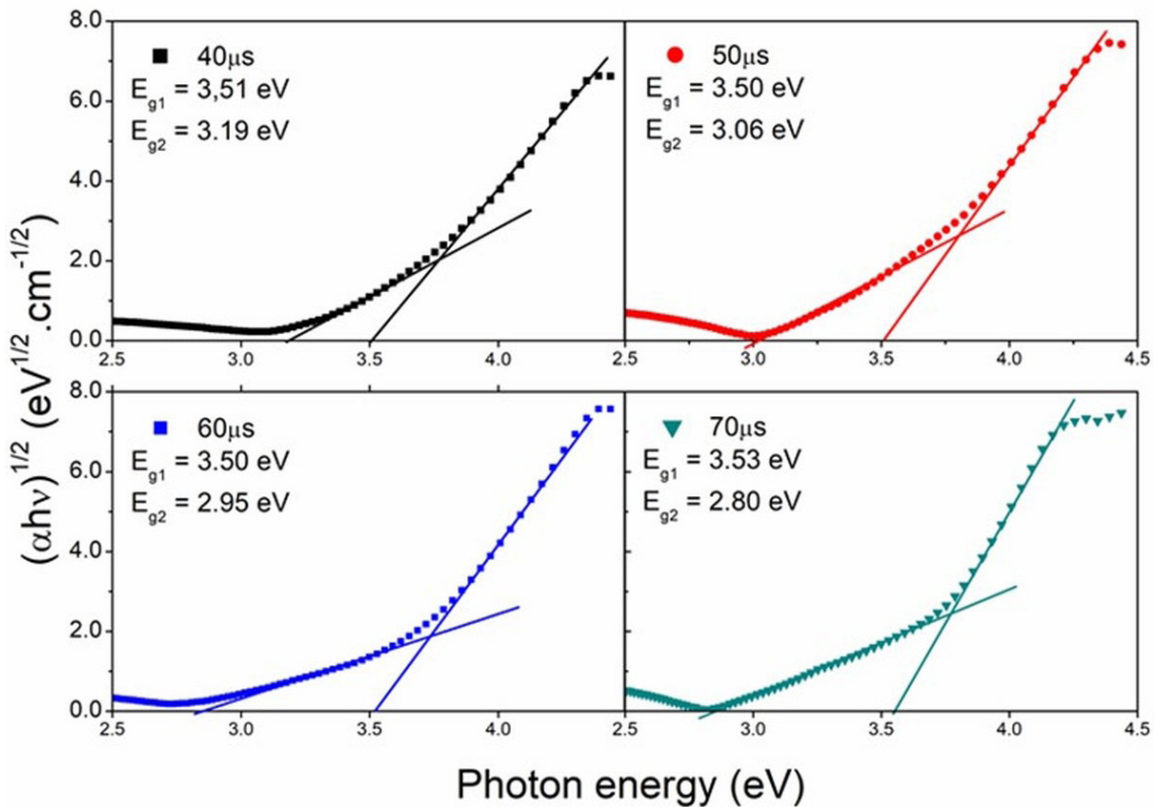
Figure 3. Transmittance for films deposited at 40  $\mu$ s, 50  $\mu$ s, 60  $\mu$ s and 70  $\mu$ s pulses.

Table 3 shows the resistivity, band gap and fractions of oxidation state for Ti obtained through van der Pauw, the Tauc method and XPS, respectively. The first band gap does not change significantly, but the film resistivity decreased down to  $10^{-4} \Omega \cdot \text{cm}$  for the 70  $\mu\text{s}$  pulse. Previous literature shows similar values for Nb:TiO<sub>2</sub> films<sup>13,29</sup>, but the authors point the need for a post-annealing treatment to reach a similar resistivity. The present method goes beyond the former ones because it makes it possible to grow low-resistivity films while keeping a high transparency in the visible range in the as-deposited condition, without the need for any post-annealing.

This can be explained by polaronic effects and electron localization affecting the materials physical and chemical properties. The nature of charge carriers in doped oxides is key to understanding the mechanism of electrical conduction in these multifunctional materials<sup>30</sup>.

Strongly dependent on their mass and size, polarons exhibit widely different conduction mechanisms, from band-like transport to thermally-activated hopping transport<sup>31,32</sup>.

XPS results show that the ratio Nb/Ti is  $0.06 \pm 0.01$  for all the films. The Figure 5 shows the XPS high-resolution spectra analysis for Ti2p which show the Ti<sup>4+</sup> oxidation state for all samples, indicating stoichiometric TiO<sub>2</sub>. The signal corresponding to the Ti<sup>3+</sup> oxidation state increases with the pulse length due to the change from oxide mode to metal mode. The fitting procedure used a Gaussian-lorentzian sum (30% lorentzian) and the background was removed through the Shirley method, using the Smart routine of the Avantage software. Spin-orbit coupling and the Coster-Kronig effect was taken into account for the fitting. The Ti<sup>3+</sup> states may be associated with the second band gap, which decreases from 3.19 eV to 2.80 eV as the pulse length increases (Table 3), in agreement with the blue-shift observed in the transmittance curves.



**Figure 4.** Band gap energy of films  $E_{g1}$  is an anatase gap with a Bursten-Moss shift and an  $E_{g2}$  as a second gap.

**Table 3.** Resistivity, band gap values and the fractions of each oxidation state for Ti in films.

$T_{\text{pulse}}$	40 $\mu\text{s}$	50 $\mu\text{s}$	60 $\mu\text{s}$	70 $\mu\text{s}$
$\rho(\Omega \text{cm})$	$(1.1 \pm 0.1) \mu 10^{-1}$	$(4.8 \pm 0.3) \mu 10^{-1}$	$(1.3 \pm 0.1) \mu 10^{-2}$	$(6.8 \pm 0.2) \mu 10^{-4}$
$E_{g1}$ (eV)	3.51	3.50	3.50	3.53
$E_{g2}$ (eV)	3.19	3.06	2.95	2.80
Ti <sup>4+</sup> (%)	96	95	90	91
Ti <sup>3+</sup> (%)	4	5	10	9

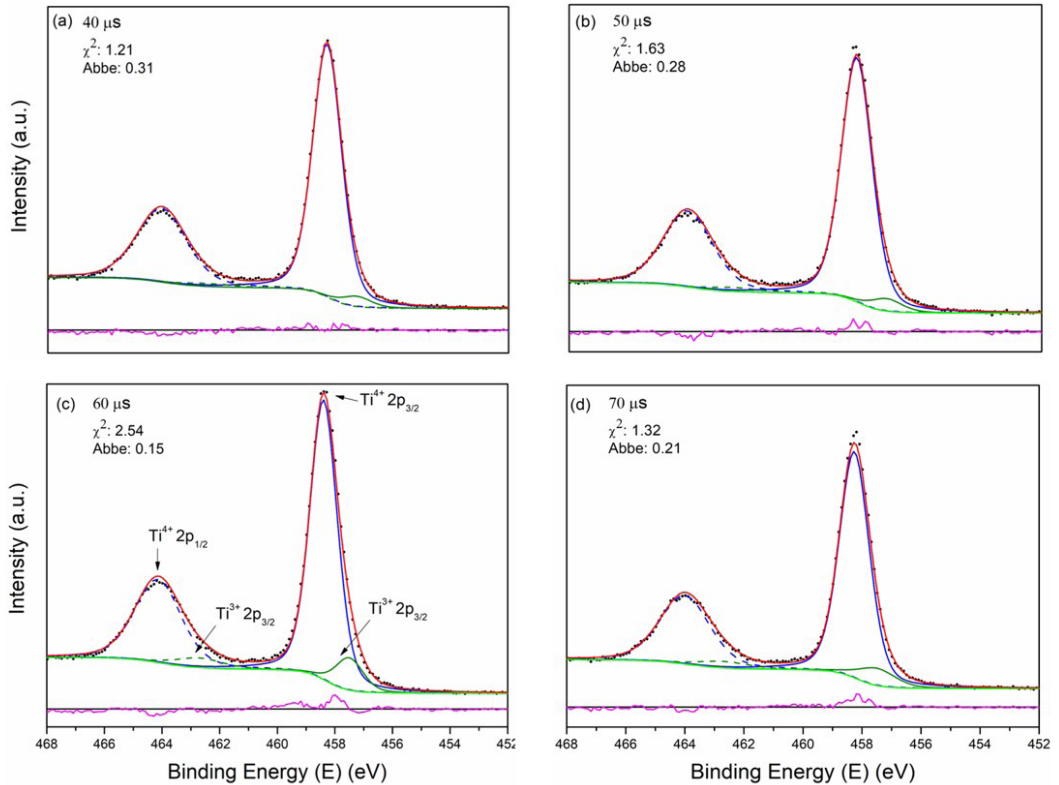


**Figure 5.** XPS peak fit analysis of Ti 2p region for films obtained through (a) 40  $\mu\text{s}$ , (b) 50  $\mu\text{s}$ , (c) 60  $\mu\text{s}$ , and (d) 70  $\mu\text{s}$  pulses. The corresponding values of normalized chi-square ( $\chi^2$ ) and Abbe criterion are shown. The residuals are plotted under the curves.

The Nb 3d spectra only show the Nb<sup>5+</sup> oxidation state. The replacing of a tetravalent Ti<sup>4+</sup> by a pentavalent Nb<sup>5+</sup> in the crystal lattice can inject an extra electron into the conduction band, thus changing the energy levels, the resistivity, and the band gap. This is the main electrical conductivity promoting factor of this compound, because the Nb impurities act as donors, resulting in an extrinsic n-type semiconducting material<sup>33</sup>. However, as the Nb/Ti ratio is almost unaffected with pulse length this can not explain the modifications in film properties with pulse length. In metal mode, there is a higher flux of Ti atoms to the film, increasing the number of Ti<sup>3+</sup> states, which collaborate to reduce the second band gap, improving the conductivity. Other effects, such as changes in film density and microstructure can not be ruled out, but need more investigations.

#### 4. Conclusions

The reactive deposition of Nb-doped TiO<sub>2</sub> films through R-HiPIMS shows that the metastable anatase phase was successfully controlled through the voltage pulse length. The “pulse length” parameter can be properly tuned so that the deposition occurs around the transition point from compound to metal mode. Consequently, the stoichiometry, the deposition rate and the properties of Nb:TiO<sub>2</sub> films (Nb/Ti=0,06±0.01), such as the resistivity and transmittance, can be controlled. Transparent, thick ( $\approx$ 500 nm) and remarkably low resistivity ( $10^{-4} \Omega\cdot\text{cm}$ ) films were obtained in the as-deposited condition for 70  $\mu\text{s}$  pulses, without the need for any post-annealing.

#### 5. Acknowledgments

This work was supported by the CAPES-PrInt grant 88881.310340/2018-01 and PRONEM/FAPESC/CNPq-2020TR730. Authors are grateful to the Mackenzie Presbyterian University, IFSC, UDESC and Filipe Estevão of Anton Paar for their support. The authors are thankful for the Multi-User Facility infrastructure from Santa Catarina State University's Technological Sciences Center.

#### 6. References

- Xiong LB, Li JL, Yang B, Yu R. Ti<sup>3+</sup> in the surface of titanium dioxide: generation, properties and photocatalytic application. *J Nanomater.* 2012(2012):831524.
- Kulczyk-Malecka J, Donaghy D, Delfour-Peyrethon B, Werner M, Chalker PR, Bradley JW, et al. Nb-doped TiO<sub>2</sub> coatings developed by high power impulse magnetron sputtering-chemical vapor deposition hybrid deposition process. *J Vac Sci Technol A.* 2020;38:033410. <https://doi.org/10.1116/6.0000118>.
- An H, Ahn HJ. Fabrication of wrinkled Nb-doped TiO<sub>2</sub> nanofibres via electrospinning. *Mater Lett.* 2013;93:88-91.
- Gudmundsson J, Lundin D, Brenning N, Raadu M, Huo C, Minea T. An ionization region model of the reactive Ar/O<sub>2</sub> high power impulse magnetron sputtering discharge. *Plasma Sources Sci Technol.* 2016;25(6):065004.
- Kadlec S, Čapek J. Return of target material ions leads to a reduced hysteresis in reactive high power impulse magnetron sputtering: model. *J Appl Phys.* 2017;121(17):171910. <http://dx.doi.org/10.1063/1.4977815>.

6. Lundin D, Minea T, Gudmundsson J. High power impulse magnetron sputtering: fundamentals, technologies, challenges and applications. USA: Elsevier Science Ltd; 2019.
7. Luo H, Gao F, Billard A. Effect of auxiliary magnetic field on the conformal coverage of the microtrenches in high power impulse magnetron sputtering. *J Mater Process Technol.* 2020;283:116732.
8. Hála M, Capek J, Zabeida O, Sapielha J, Martinu L. Hysteresis-free deposition of niobium oxide films by HiPIMS using different pulse management strategies. *J Phys D Appl Phys.* 2012;45(5):055204.
9. Anders A. Tutorial: reactive high power impulse magnetron sputtering (R-HiPIMS). *J Appl Phys.* 2017;121(17):171101.
10. Ganesan R, Murdoch B, Treverrow B, Ross A, Falconer I, Kondyurin A, et al. The role of pulse length in target poisoning during reactive HiPIMS: application to amorphous HfO<sub>2</sub>. *Plasma Sources Sci Technol.* 2015;24(3):035015.
11. Ganesan R, Treverrow B, Murdoch B, Xie D, Ross A, Partridge J, et al. Duty cycle control in reactive high-power impulse magnetron sputtering of hafnium and niobium. *J Phys D Appl Phys.* 2016;49:245201.
12. Yamada N, Hitosugi T, Hoang N, Furubayashi T, Hirose Y, Konuma S, et al. Structural, electrical and optical properties of sputter-deposited Nb-doped TiO<sub>2</sub> (TNO) polycrystalline films. *Thin Solid Films.* 2008;516(17):5754-7.
13. Castro M, Rebouta L, Alpuim P, Cerqueira M, Benelmekki M, Garcia C, et al. Optimisation of surface treatments of TiO<sub>2</sub>:Nb transparent conductive coatings by a post-hot-wire annealing in a reducing H<sub>2</sub> atmosphere. *Thin Solid Films.* 2014;550:404-12.
14. Tauc JR, Grigorovici A, Vancu A. Optical properties and electronic structure of amorphous germanium. *Phys Status Solidi, B Basic Res.* 1966;15(2):627-37.
15. Pauw L. A method of measuring the resistivity and hall coefficient on lamellae of arbitrary shape. *Philips Tech. Rev.* 1958;20:220-4.
16. Kubart T, Aijaz A. Evolution of sputtering target surface composition in reactive high power impulse magnetron sputtering. *J Appl Phys.* 2017;121(17):171903.
17. Depla D, Heirwegh S, Mahieu S, Haemers J, Gryse R. Understanding the discharge voltage behavior during reactive sputtering of oxides. *J Appl Phys.* 2007;101(1):013301.
18. Wojcieszak D, Mazur M, Kaczmarek D, Poniedzialek A, Domanowski P, Szponar B, et al. Effect of the structure on biological and photocatalytic activity of transparent titania thin-film coatings. *Mater Sci Pol.* 2016;34(4):856-62.
19. Fox M. Optical properties of solids, New York: Oxford University Press; 2001.
20. Samat M, Ali TAIB, Taib MFM, Hassan OH, Yahya MZA. Hubbard U calculations on optical properties of 3d transition metal oxide TiO<sub>2</sub>. *Results Phys.* 2016;6:891-6.
21. Zhang L, Ran J, Quiao S, Jaroniec M. Characterization of semiconductor photocatalysts. *Chem Soc Rev.* 2019;48(20):5184-206.
22. Zubair M, Mamun A, Mcnamara K, Tofail S, Islam F, Lebedev V. Amorphous interface oxide formed due to high amount of Sm doping (5-20 mol%) stabilizes finer size anatase and lowers indirect band gap. *Appl Surf Sci.* 2020;529:146967.
23. Diebold U. The surface science of titanium dioxide. *Surf Sci Rep.* 2003;48(5-8):53-229.
24. Zhang Y, Xu X. Machine learning band gaps of Doped-TiO<sub>2</sub> photocatalysts from structural and morphological parameters. *ACS Omega.* 2020;5(25):15344-52.
25. Sato Y, Akizuki H, Kamiyama T, Shigesato Y. Transparent conductive Nb-doped TiO<sub>2</sub> films deposited by direct-current magnetron sputtering using a TiO<sub>2</sub> - x target. *Thin Solid Films.* 2008;516(17):5758-62.
26. Hung K, Lee P, Hsu W, Hsing H, Chang H, Wong M. Transparent conducting oxide films of heavily Nb-doped titania by reactive co-sputtering. *J Alloys Compd.* 2011;509(42):10190-94.
27. Setvin M, Franchini C, Hao X, Schmid M, Janotti A, Kaltak M, et al. Direct view at excess electrons in TiO<sub>2</sub> rutile and anatase. *Phys Rev Lett.* 2014;113(8):086402.
28. Mardare D, Yildiz A, Girtan M, Manole A, Dobromir M, Irimia M, et al. Surface wettability of titania thin films with increasing Nb content. *J Appl Phys.* 2012;112(7):073502.
29. Jiang C, Wu Z, Xiao S, Ma Z, Liu L, Fu R, et al. Structural and optoelectrical properties of Nb-TiO<sub>2</sub> films fabricated by low-energy magnetron sputtering and post-annealing. *Surf Coat Technol.* 2019;365:10-4.
30. Verdi C, Caruso F, Giustino F. Origin of the crossover from polarons to Fermi liquids in transition metal oxides. *Nat Commun.* 2017;8(1):15769.
31. Austin I, Mott N. Polarons in crystalline and non-crystalline materials. *Adv Phys.* 1969;18(71):41-102.
32. Ziman J. Electrons and phonons. Cary: Oxford University Press; 1960.
33. Yildiz A, Mardare D. Polaronic transport in TiO<sub>2</sub> thin films with increasing Nb content. *Philos Mag.* 2011;91(34):4401-9.